



Indications for a critical point in the phase diagram for hot and dense nuclear matter

Roy A. Lacey

Depts. of Chemistry & Physics, Stony Brook University, NY 11794

Abstract

Two-pion interferometry measurements are studied for a broad range of collision centralities in Au+Au ($\sqrt{s_{NN}} = 7.7 - 200$ GeV) and Pb+Pb ($\sqrt{s_{NN}} = 2.76$ TeV) collisions. They indicate non-monotonic excitation functions for the Gaussian emission source radii difference ($R_{\text{out}}^2 - R_{\text{side}}^2$), suggestive of reaction trajectories which spend a fair amount of time near a soft point in the equation of state (EOS) that coincides with the critical end point (CEP). A Finite-Size Scaling (FSS) analysis of these excitation functions, provides further validation tests for the CEP. It also indicates a second order phase transition at the CEP, and the values $T^{\text{cep}} \sim 165$ MeV and $\mu_B^{\text{cep}} \sim 95$ MeV for its location in the (T, μ_B) -plane of the phase diagram. The static critical exponents ($\nu \approx 0.66$ and $\gamma \approx 1.2$) extracted via the same FSS analysis, place this CEP in the 3D Ising model (static) universality class. A Dynamic Finite-Size Scaling analysis of the excitation functions, gives the estimate $z \sim 0.87$ for the dynamic critical exponent, suggesting that the associated critical expansion dynamics is dominated by the hydrodynamic sound mode.

Keywords: critical point, phase transition, static critical exponents, dynamic critical exponent

1. Introduction

A major goal of the worldwide program in relativistic heavy ion research, is to chart the phase diagram for nuclear matter [1, 2, 3, 4]. Pinpointing the location of the phase boundaries and the critical end point (CEP), in the plane of temperature (T) versus baryon chemical potential (μ_B), is key to this mapping. Full characterization of the CEP not only requires its location, but also the static and dynamic critical exponents which classify its critical dynamics and thermodynamics, and the order of the associated phase transition.

Current theoretical guidance indicates that the CEP belongs to the 3D-Ising [or Z(2)] static universality class with the associated critical exponents $\nu \approx 0.63$ and $\gamma \approx 1.2$ [4, 5]. However, the predictions for its location span a broad swath of the (T, μ_B) -plane, and do not provide a consensus on its location [4]. A recent study which takes account of the non-linear couplings of the conserved densities [6] suggests that the CEP's critical dynamics may be controlled by three distinct slow modes, each characterized by a different value of the dynamic critical exponent z ; a thermal mode ($z_T \sim 3$), viscous mode ($z_v \sim 2$) and a sound mode ($z_s \sim -0.8$). The phenomena of critical slowing down results from $z > 0$. The predicted negative value for z_s could have profound implications for the CEP search since it implies critical speeding-up for critical reaction dynamics involving *only* the sound mode. The present-day theoretical challenges emphasize the need for detailed experimental validation and characterization of the CEP.

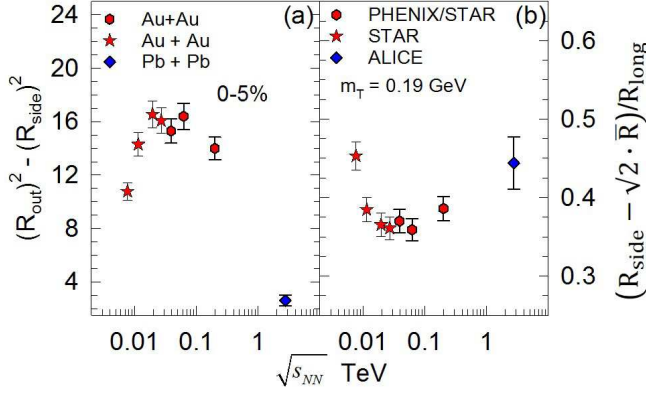


Fig. 1: (Color online) The $\sqrt{s_{NN}}$ dependence of (a) $(R_{out}^2 - R_{side}^2)$, and (b) $[(R_{side} - \sqrt{2}\bar{R})/R_{long}]$ [8].

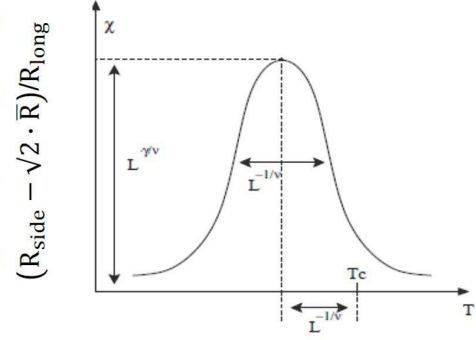


Fig. 2: Illustration of the Finite-Size (L) dependence of the peak position, width and magnitude of the susceptibility χ (see text).

2. Anatomy of the search strategy for the CEP

The critical point is characterized by several (power law) divergences linked to the divergence of the correlation length $\xi \propto |t|^{-\nu} \equiv |T - T^{cep}|^{-\nu}$. Notable examples are the baryon number fluctuations $\langle\langle \delta n \rangle\rangle \sim \xi^{\gamma/\nu}$, the isobaric heat capacity $C_p \sim \xi^{\gamma/\nu}$ and the isothermal compressibility $\kappa_T \sim \xi^{\gamma/\nu}$. Such divergences suggest that reaction trajectories which are close to the CEP, could drive anomalies in the reaction dynamics to give distinct non-monotonic patterns for the related experimental observables. Thus, a current experimental strategy is to carry out beam energy scans which enable a search for non-monotonic excitation functions over a broad domain of the (T, μ_B) -plane. In this work we use the non-monotonic excitation functions for HBT radii combinations that are sensitive to the divergence of the compressibility [7].

The expansion of the pion emission source produced in heavy ion collisions, is driven by the sound speed $c_s^2 = 1/\rho\kappa_s$, where ρ is the density, $\kappa_s = \zeta\kappa_T$ is the isentropic compressibility and $\zeta = C_v/C_p$ is the ratio of the isochoric and isobaric heat capacities. Thus, an emitting source produced in the vicinity of the CEP, would be subject to a precipitous drop in the sound speed and the collateral increase in the emission duration [9], which results from the divergence of the compressibility. The space-time information associated with these effects, are encoded in the Gaussian HBT radii which serve to characterize the emission source. That is, R_{long} is related to the source lifetime τ , $(R_{out}^2 - R_{side}^2)$ is sensitive to its emission duration $\Delta\tau$ [10] (an intensive quantity) and $[(R_{side} - \sqrt{2}\bar{R})/R_{long}]$ gives an estimate for its expansion speed (for small values of m_T), where \bar{R} is an estimate of the initial transverse size, obtained via Monte Carlo Glauber model calculations [8, 7]. Therefore, characteristic convex and concave shapes are to be expected for the non-monotonic excitation functions for $(R_{out}^2 - R_{side}^2)$ and $[(R_{side} - \sqrt{2}\bar{R})/R_{long}]$ respectively.

These predicted patterns are validated in Figs. 1(a) and (b). They reinforce the connection between $(R_{out}^2 - R_{side}^2)$ and the compressibility and suggest that reaction trajectories spend a fair amount of time near a soft point in the EOS that coincides with the CEP. We associate $(R_{out}^2 - R_{side}^2)$ with the susceptibility κ and employ Finite-Size Scaling (FSS) for further validation tests, as well as to extract estimates for the location of the CEP and the critical exponents which characterize its static and dynamic properties.

3. Characterization of the CEP via Finite-Size Scaling

For infinite volume systems, ξ diverges near T^{cep} . Since $\xi \leq L$ for a system of finite size L^d (d is the dimension), only a pseudo-critical point, shifted from the genuine CEP, is observed. This leads to a characteristic set of Finite-Size Scaling (FSS) relations for the magnitude (χ_T^{max}), width (δT) and peak position (t_T) of the susceptibility [7] as illustrated in Fig. 2; $\chi_T^{max}(V) \sim L^{\gamma/\nu}$, $\delta T(V) \sim L^{-1/\nu}$ and $t_T(V) \sim$

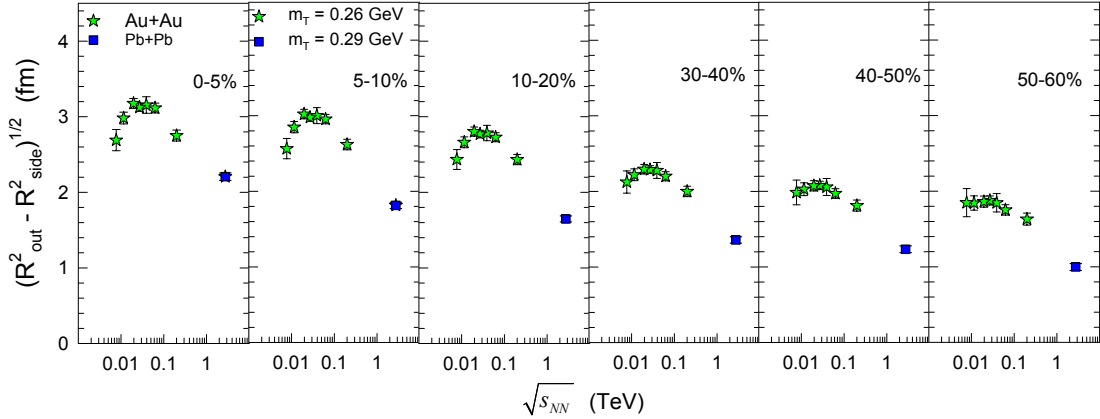


Fig. 3: (Color online) $(R_{\text{out}}^2 - R_{\text{side}}^2)^{1/2}$ vs. $\sqrt{s_{NN}}$ for 0-5%, 5-10%, 10-20%, 30-40%, 40-50% and 50-60% Au+Au and Pb+Pb collisions for $m_T = 0.26$ GeV and 0.29 GeV respectively [7].

$T^{\text{cep}}(V) - T^{\text{cep}}(\infty) \sim L^{-1/\nu}$. It also leads to the scaling function $\chi(T, L) = L^{\gamma/\nu} P_\chi(tL^{1/\nu})$, which results in data collapse onto a single curve.

These scaling relations indicate that even a flawless measurement can not give the precise location of the CEP if it is subject to Finite-Size Effects (FSE) (a crucial point which is often missed or ignored). However, they point to specific identifiable dependencies on size (L) which can be leveraged via FSS, to estimate the location of the CEP and its associated critical exponents [7].

Such dependencies can be observed in Fig. 3 where a representative set of excitation functions, obtained for the broad selection of centrality cuts, are shown. They indicate that (i) the magnitude of the peaks decrease with increasing centrality (%) or decreasing transverse size, (ii) the positions of the peaks shift to lower values of $\sqrt{s_{NN}}$ with an increase in centrality and (iii) the width of the distributions grow with centrality. A Gaussian fit was used to extract the peak positions, and widths of the excitation functions, for different system sizes characterized by the centrality selections indicated in Fig. 3; the magnitude of $(R_{\text{out}}^2 - R_{\text{side}}^2)$ was evaluated at the extracted peak positions as well. A subsequent FSS analysis (with $L = \bar{R}$), of these peak positions, widths and magnitudes was used to obtain estimates for the critical exponents ν and γ and the infinite volume $\sqrt{s_{NN}}(\infty)$ value where the de-confinement phase transition first occurs; $(R_{\text{out}}^2 - R_{\text{side}}^2)^{\text{max}} \propto \bar{R}^{\gamma/\nu}$, and $\sqrt{s_{NN}}(V) = \sqrt{s_{NN}}(\infty) - k \times \bar{R}^{-1/\nu}$. k is a constant and $\delta s \equiv (\sqrt{s} - \sqrt{s^{\text{cep}}}) / \sqrt{s^{\text{cep}}}$ gives a measure of the ‘‘distance’’ to the CEP.

Figure 4 illustrates the FSS test made for the extracted peak positions ($\sqrt{s_{NN}}(V)$). The dashed curve in (b), which represents a fit to the data in (a), confirms the expected inverse power law dependence of these peaks on \bar{R} . The fit gives the values $\sqrt{s_{NN}}(\infty) = 47.5 \pm 1.5$ GeV and $\nu = 0.67 \pm 0.05$. The same value for ν was obtained via an analysis of the widths. The estimate $\gamma = 1.15 \pm 0.065$, was obtained from FSS of the the magnitudes of the excitation functions. The extracted values for the critical exponents indicate that the deconfinement phase transition at the CEP is second order, and places it in the 3D Ising model (static) universality class. The extracted value $\sqrt{s_{NN}}(\infty) = 47.5$ GeV was used in conjunction with the parametrization for chemical freeze-out in Ref. [11], to obtain the estimates $\mu_B^{\text{cep}} \sim 95$ MeV and $T^{\text{cep}} \sim 165$ MeV for its location in the (T, μ_B) -plane.

A crucial crosscheck for the location of the CEP and its associated critical exponents, is to use the FSS function to demonstrate data collapse onto a single curve for the extracted values of T^{cep} , μ_B^{cep} and the critical exponents ν and γ ; $\bar{R}^{-\gamma/\nu}(R_{\text{out}}^2 - R_{\text{side}}^2)$ vs. $\bar{R}^{1/\nu} t_T$ and $\bar{R}^{-\gamma/\nu}(R_{\text{out}}^2 - R_{\text{side}}^2)$ vs. $\bar{R}^{1/\nu} t_{\mu_B}$ where $t_T = (T - T^{\text{cep}}) / T^{\text{cep}}$ and $t_{\mu_B} = (\mu_B - \mu_B^{\text{cep}}) / \mu_B^{\text{cep}}$ are the reduced temperature and baryon chemical potential respectively. The efficacy of this crosscheck is illustrated in Fig. 5 where data collapse onto a single curve is indicated for the RHIC excitation functions shown in Fig. 3. Here, the parametrization for chemical freeze-out [11] was used in conjunction with μ_B^{cep} and T^{cep} to determine the required t_T and t_{μ_B} values from the $\sqrt{s_{NN}}$ values plotted in Fig. 3. Figs. 5(a) and (b) also validate the expected trends for reaction trajectories in the (T, μ_B) domain which encompass the CEP. That is, the scaled values of $(R_{\text{out}}^2 - R_{\text{side}}^2)$ peaks at $t_T \approx 0$ and $t_{\mu_B} \approx 0$, and show

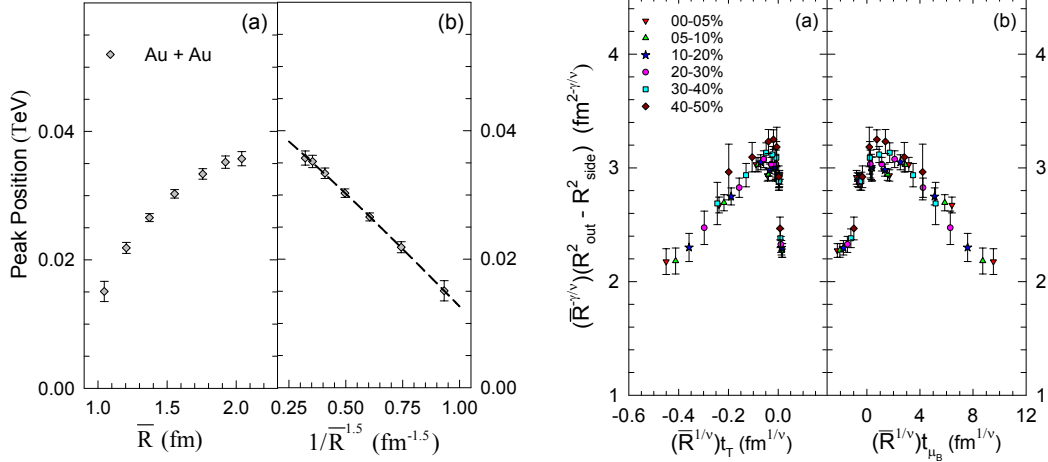


Fig. 4: (Color online) (a) Peak position vs. \bar{R} . (b) Peak position vs. $1/\bar{R}^{1.5}$. The dashed curve in (b) shows the fit to the data in (a).

Fig. 5: (Color online) (a) $\bar{R}^{-\gamma/\nu}(R_{\text{out}}^2 - R_{\text{side}}^2)$ vs. $\bar{R}^{1/\nu}t_T$. (b) $\bar{R}^{-\gamma/\nu}(R_{\text{out}}^2 - R_{\text{side}}^2)$ vs. $\bar{R}^{1/\nu}t_{\mu_B}$.

the collateral fall-off for $t_{T,\mu_B} < 0$ and $t_{T,\mu_B} > 0$.

The susceptibility diverges at the CEP, so relaxation of the order parameter could be anomalously slow, *i.e.* $\tau \sim \xi^z$, where z is the dynamic critical exponent. Such an anomaly can lead to significant attenuation of the signals associated with the CEP ($\xi \sim \tau^{1/z}$) for critical dynamics driven by the thermal ($z_T \sim 3$) and viscous ($z_v \sim 2$) slow modes, especially for the short-lived processes of interest. This phenomena of critical slowing down would switch to critical speeding up for critical dynamics driven by the sound mode ($z_s \sim -0.8$). Thus, a rudimentary knowledge of the magnitude and the sign of the dynamic critical exponent/s can significantly enhance experimental studies of the CEP. The Dynamic Finite Size scaling function can be expressed as; $\chi(L, T, \tau) = L^{\gamma/\nu} f(L^{1/\nu} t_T, \tau L^{-z})$. For $T \sim T^{\text{cep}}$ it simplifies to the expression $\chi(L, T, \tau) = L^{\gamma/\nu} f(\tau L^{-z})$ which is observed to scale the data for $\bar{R}^{-\gamma/\nu}(R_{\text{out}}^2 - R_{\text{side}}^2)$ vs. $R_{\text{long}} \bar{R}^{-z}$ and give the estimate $z \sim 0.87$. Here, R_{long} is used as a proxy for τ .

In summary, we have investigated the centrality dependent excitation functions for the Gaussian emission source radii difference ($R_{\text{out}}^2 - R_{\text{side}}^2$), obtained from two-pion interferometry measurements in Au+Au ($\sqrt{s_{NN}} = 7.7 - 200$ GeV) and Pb+Pb ($\sqrt{s_{NN}} = 2.76$ TeV) collisions, to characterize the CEP. The observed centrality dependent non-monotonic excitation functions, validate characteristic finite-size scaling patterns that are consistent with a deconfinement phase transition and the critical end point. A Finite-Size Scaling analysis of these data indicates a second order phase transition at a CEP located at $T^{\text{cep}} \sim 165$ MeV and $\mu_B^{\text{cep}} \sim 95$ MeV in the (T, μ_B) -plane of the phase diagram. The critical exponents ($\nu = 0.67 \pm 0.05$ and $\gamma = 1.15 \pm 0.065$) extracted in the same FSS analysis, places the CEP in the 3D Ising model (static) universality class. An initial estimate of $z \sim 0.87$ for the dynamic critical exponent is incompatible with the commonly assumed Model H dynamic universality class ($z \sim 3$) assigned to critical expansion dynamics.

References

- [1] N. Itoh, Prog. Theor. Phys. 44 (1970) 291–292.
- [2] E. V. Shuryak, CERN-83-01 (1983) 1.
- [3] M. Asakawa, K. Yazaki, Nucl. Phys. A504 (1989) 668–684.
- [4] M. A. Stephanov, K. Rajagopal, E. V. Shuryak, Phys. Rev. Lett. 81 (1998) 4816–4819. arXiv:hep-ph/9806219.
- [5] The critical exponents satisfy several equalities. Thus, only two of the four exponents are independent.
- [6] Y. Minami, Phys. Rev. D83 (2011) 094019. arXiv:1102.5485, doi:10.1103/PhysRevD.83.094019.
- [7] R. A. Lacey, Phys. Rev. Lett. 114 (14) (2015) 142301. arXiv:1411.7931, doi:10.1103/PhysRevLett.114.142301.
- [8] R. A. Lacey, Nucl. Phys. A931 (2014) 904–909. arXiv:1408.1343, doi:10.1016/j.nuclphysa.2014.10.036.

- [9] D. H. Rischke, M. Gyulassy, Nucl.Phys. A608 (1996) 479–512. [arXiv:nucl-th/9606039](#), [doi:10.1016/0375-9474\(96\)00259-X](#).
- [10] T. Csorgo, B. Lorstad, Phys. Rev. C54 (1996) 1390–1403. [arXiv:hep-ph/9509213](#), [doi:10.1103/PhysRevC.54.1390](#).
- [11] J. Cleymans, H. Oeschler, K. Redlich, S. Wheaton, J.Phys. G32 (2006) S165–S170. [arXiv:hep-ph/0607164](#), [doi:10.1088/0954-3899/32/12/S21](#).



ELSEVIER